Wind Speed Measurement from Bistatically Scattered GPS Signals

James L. Garrison, Attila Komjathy, , Valery U. Zavorotny, Stephen J. Katzberg

Abstract

Instrumentation and retrieval algorithms are described which use the forward, or bistatically scattered range-coded signals from the Global Positioning System (GPS) radio navigation system for the measurement of sea surface roughness. This roughness is known to be related directly to the surface wind speed. Experiments were conducted from aircraft along the TOPEX ground track, and over experimental surface truth buoys. These flights used a receiver capable of recording the cross correlation power in the reflected signal. The shape of this power distribution was then compared against analytical models derived from geometric optics. Two techniques for matching these functions were studied. The first recognized the most significant information content in the reflected signal is contained in the trailing edge slope of the waveform. The second attempted to match the complete shape of the waveform by approximating it as a series expansion and obtaining the nonlinear least squares estimate. Discussion is also presented on anomalies in the receiver operation and their identification and correction.

Keywords

J. Garrison is with NASA Goddard Space Flight Center, Code 572, Greenbelt, MD, 20707, E-mail: jgarriso@pop500.gsfc.nasa.gov

A. Komjathy is with the Colorado Center for Astrodynamics Research, Campus Box 431, University of Colorado, Boulder, CO, 80309-0431, E-mail: komjathy@GPS.colorado.edu

V. Zavorotny is with the CIRES/NOAA Environmental Technology Laboratory, R/E/ET6, 325 Broadway, Boulder, CO, 80303-3328, E-mail: vzavorotny@etl.noaa.gov

S. Katzberg is with NASA Langley Research Center, Mail Stop 328, Hampton, VA, 23681, E-mail: s.j.katzberg@larc.nasa.gov

Global Positioning System (GPS), Scatterometry, Oceanography, Retrievals

I. Introduction

IT has long been recognized that the reflection of electromagnetic radiation from the ocean surface contains information about the statistical properties of that surface. These statistics are indirectly related to the near-surface meteorological conditions. This relationship forms the basis of most oceanographic radar remote sensing systems. Most experiments to date, however, have used systems employing a dedicated transmitter and receiver. Furthermore, these systems have almost always been monostatic, measuring the power of the backscattered radiation. The possibility of using the radio navigation signals from the Global Positioning System (GPS) as a source of illumination in a bistatic, or forward scattered radar remote sensing instrument for sea surface roughness was first disclosed in a 1998 patent application [1]. This invention was unique, not only in the use of a bistatic geometry with existing sources of radio frequency illumination, but also in the application of the correlation properties of the pseudo random noise signal transmitted by GPS.

Katzberg et. al's, patent application proposed measuring the shape of the cross correlation between a reflected signal and the locally generated pseudorandom noise (PRN) code. This paper documents the subsequent research performed to mechanize this instrument concept, involving the construction of a specialized GPS receiver and the inversion of bistatic scattering models to estimate wind speed from correlation measurements. The conduct of two campaigns of aircraft flights in conjunction with surface truth and satellite remote sensing measurement and one high altitude balloon experiment are described.

II. Experiment Description

A. Measurement Technique

CONSIDER first the reflection of a GPS signal from a perfectly flat conducting surface. Other than a change in polarization from exclusively right hand circular to predominantly left hand circular (which can be accounted for with a proper antenna design), the reflected signal will appear identical to a direct signal delayed by the path length difference to the specular point. Consequently when the cross-correlation between this signal and the locally generated PRN code is computed as a function of the relative delay between the two signals, it will ideally be described by the function

$$\Lambda(\delta) = \left\{ \begin{array}{cc} 1 - \left|\frac{\delta}{\delta_C}\right| & -\delta_C \leq \delta \leq \delta_C \\ 0 & otherwise \end{array} \right\} \tag{1}$$

in which δ is the relative delay (in distance) between two codes, and δ_C is the length of one code "chip" or data bit transition (300 meters for the C/A code used exclusively in this experimentation). For more details on the fundamentals of GPS receiver technology the interested reader is referred to several textbook references [2] and [3]. Given the incoherent nature of the reflected signal, it is best to work only with power, not voltage signals, therefore the square of this function, $\Lambda^2(\delta)$ is used from now on.

When the surface is not perfectly flat, but has some random variation in height, then the incident radiation will be reflected from points having longer path length delays than the specular point. The result of this is that all of the reflected signal power no longer arrives with a single time delay, but rather with a continuous distribution in delay. When the cross correlation is performed, the result will

therefore be an infinite sum of the Λ^2 functions at these delays, scaled with the relative power density. This sum can be expressed as a convolution of the reflected power distribution with the Λ^2 function.

$$Y^2(\delta) = \int p(\eta)\Lambda^2(\delta - \eta)d\eta \tag{2}$$

The power per unit delay, $p(\eta)$ is itself computed by the integral of reflected power over all points with delay η. (The locus of these points forms an ellipse on a flat reflecting surface).

Qualitatively, the reflecting surface roughness increases with increasing surface wind speed. Analytical and empirical models have been generated for this dependence [4], [5] and [6]. The application of them for the retrieval of wind speed will be described later in this paper.

B. Instrumentation

A GPS receiver development system [7] was used to make the first experimental measurements of reflected GPS signals. Software was written for this receiver board to allow direct open-loop control of the correlator code delay and the down conversion frequency for a set of correlator channels operating on the 2 bit digitized signal from a downward-looking left hand circularly polarized (LHCP) antenna. An automatic gain control (AGC) is used prior to this digitization to set the statistics of the noise-like signal prior to correlation. This receiver was capable of tracking direct line of sight satellites through a zenith-oriented right hand circularly polarized (RHCP) antenna and recording the cross-correlation function from the same six satellites viewed as reflected signals using a nadir-oriented LHCP antenna.

The Serial Delay Mapping Receiver (SDMR), illustrated in figure 1 tracks up to 6 direct satellites and generates a position and time solution from their pseudroanges. This position is used to initialize

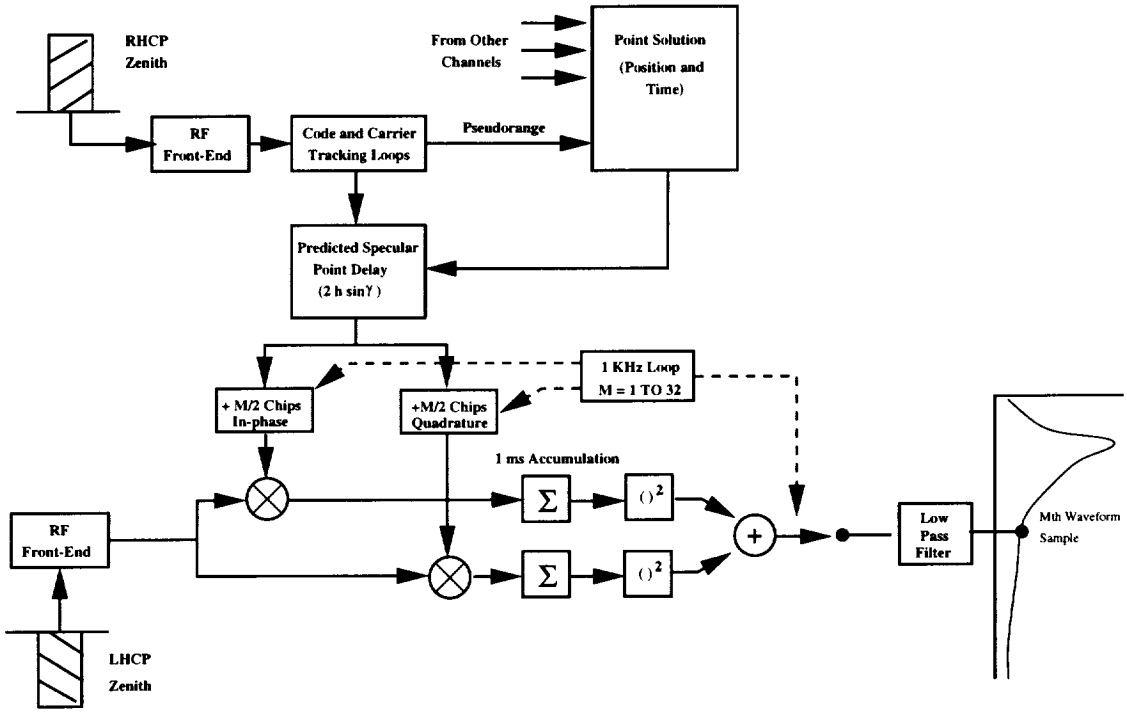

Fig. 1. Serial Delay Mapping Receiver (SDMR)

the code delay and Doppler frequency in the reflected channels. The code delay is set to approximate a specular reflection delay of $2h\sin(\gamma)$ within the nearest half code chip. (h is the receiver altitude over a flat Earth and γ is the reflection grazing angle.) It then records the correlation power from the reflected signal in 32 range bins for each of the same 6 satellites by sequentially stepping through relative delays and performing a coherent integrating of the in-phase and quadrature components for 1 ms at each step. The correlation power is then computed as the sum square of these two components. This power in each range bin is passed through a moving average filter with a time constant of 1 second and then saved to disk once per second. The commanded code delay of each reflected channel correlator relative to that for the direct (tracking) channel is also saved.

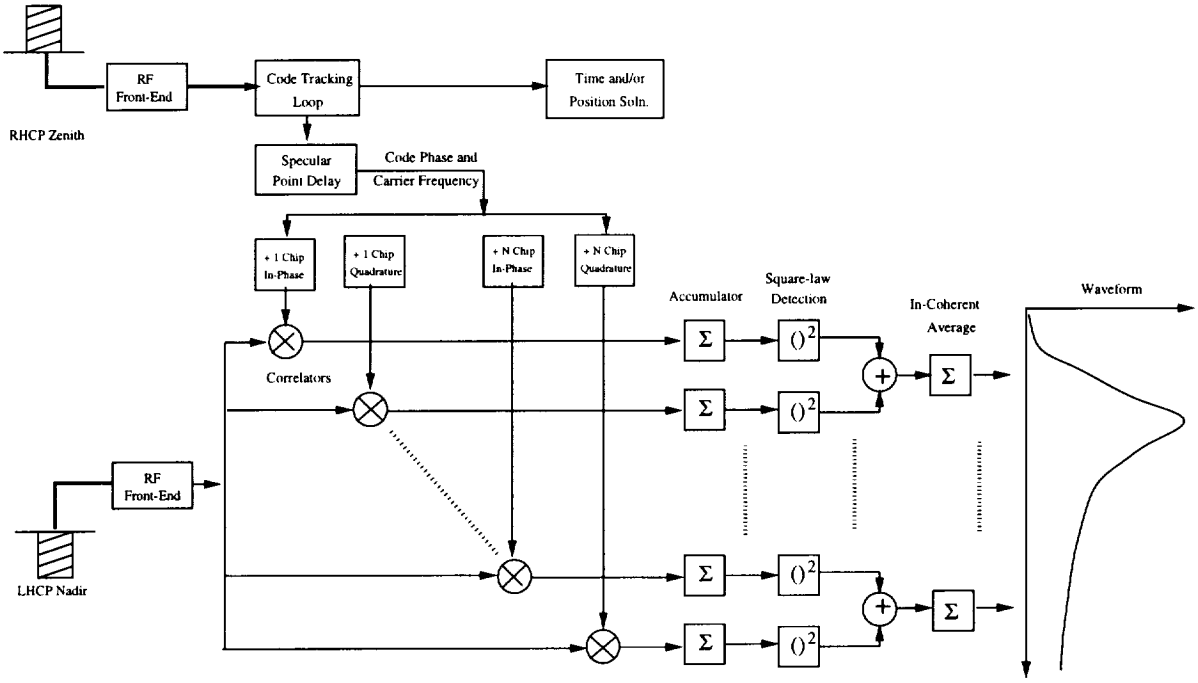

Fig. 2. Parallel Delay Mapping Receiver (PDMR)

This instrumentation was improved, entirely through software enhancements, to continuously record the cross-correlation in 10 to 12 range bins at fixed delays all from one or two satellites. The coherent integration time is fixed at 1 ms on the correlator chip hardware. However, the sum square of the inphase and quadrature components is (incoherently) averaged for 0.1 seconds before being saved to disk. Furthermore, samples of the relative code phase between the direct and reflected channels are taken at each 0.1 second interval. This improves the ability to reference the waveform samples to specular point delays. This Parallel Delay Mapping Receiver (PDMR), illustrated in figure 2, has an improvement in signal to noise ratio of 10 dB over the SDMR at each sample.

In the PDMR, the timing differences between the direct channel and the parallel reflected channels is measured each 0.1 second to a precision of 1/2048 chip. Although the samples are still placed at half

code chip spacing, this knowledge of the timing allows subsequent samples to be better aligned with the true estimate of the specular point, taking out much of the error resulting from aircraft motion. Previously, the placement of samples could only be known to a precision of 1/4 code chip and the results were averaged in 1/2 chip bins.

C. Data Collection Campaigns

The first collection of correlation data from reflected GPS signals occurred on four aircraft flights between July and November, 1997. These early experiments compared measured waveform shapes collected under a variety of sea state conditions (as measured by NOAA NDBC buoys) [8].

Two aircraft flight campaigns were flown using this receiver in conjunction with surface truth measurements and other remote sensing instrumentation. The purpose of these experiments was to provide comparison data for wind speed retrievals from the reflected GPS signal. The NASA Goddard Space Flight Center C-130 aircraft operating out of the NASA Wallops Flight Facility was flown along the TOPEX-Poseidon ground track (cycles no. 107, 110 and 111, pass no. 228) on three different days (on May 5, June 6, and Jun 15, 1998) and the B-200 King Air aircraft from NASA Langley Research Center was flown along along this same track on a different day (Dec. 7, 1999). These flights offered the first direct comparison between cross-correlation measurement from the delay-mapping receivers and existing instruments.

Later, the B-200 aircraft was used in conjunction with the Space and Naval Warfare Systems Command (SPAWAR) Electro-Optical Propagation Assessment in Coastal Environments (EOPACE) program, sponsored by the Office of Naval Research (ONR). These flight experiments took place off the

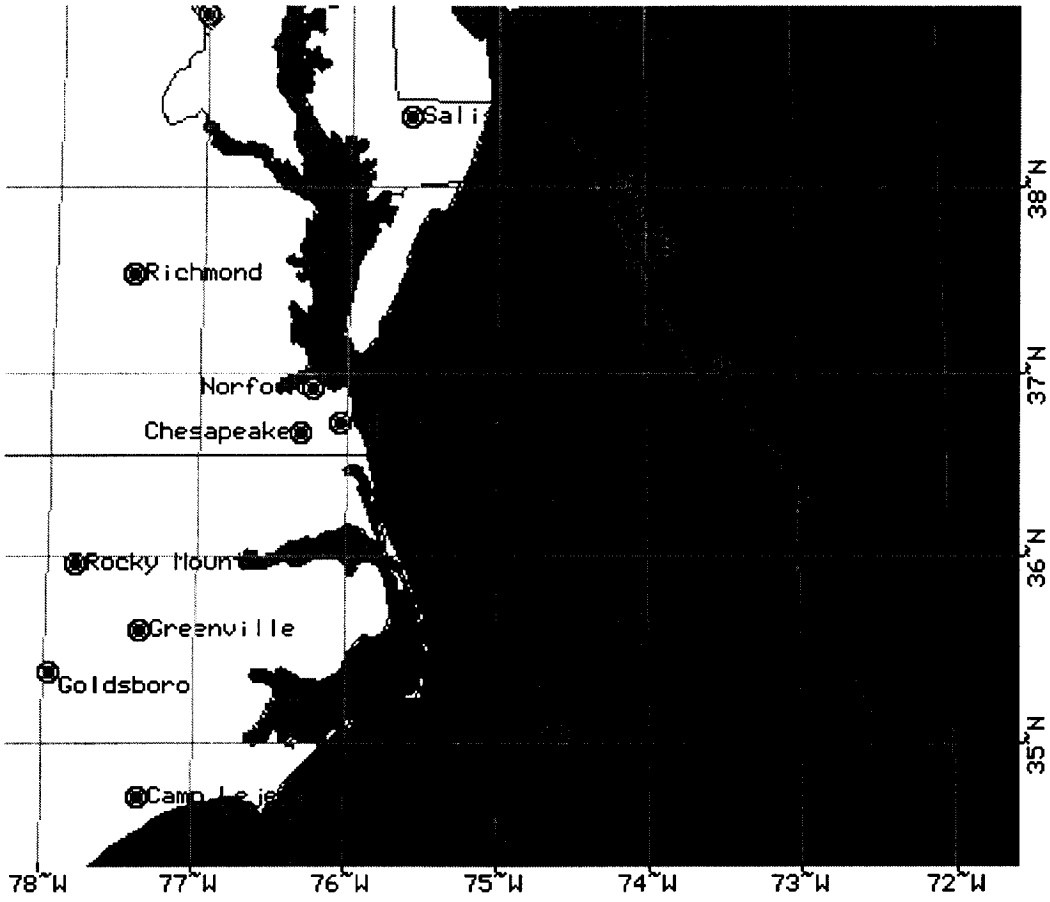

Fig. 3. TOPEX Experiment Flight Path

coast of Duck, NC. on five different days (Mar. 1, 5, 8, 11 and 12, 1999) along the same ground track. Surface truth data was available at three different locations: the Duck meteorological station (DUCN7), and two research buoys provided for this experiment (identified as the "Flux" and "Met" buoy).

The flight path of the TOPEX underflight is shown in figure 3, and that of the EOPACE experiments is shown in figure 4. Figure 4 also shows the location of 3 data buoys.

On August 22, 1998, the SDMR hardware was carried to altitudes in excess of 25 km on a balloon

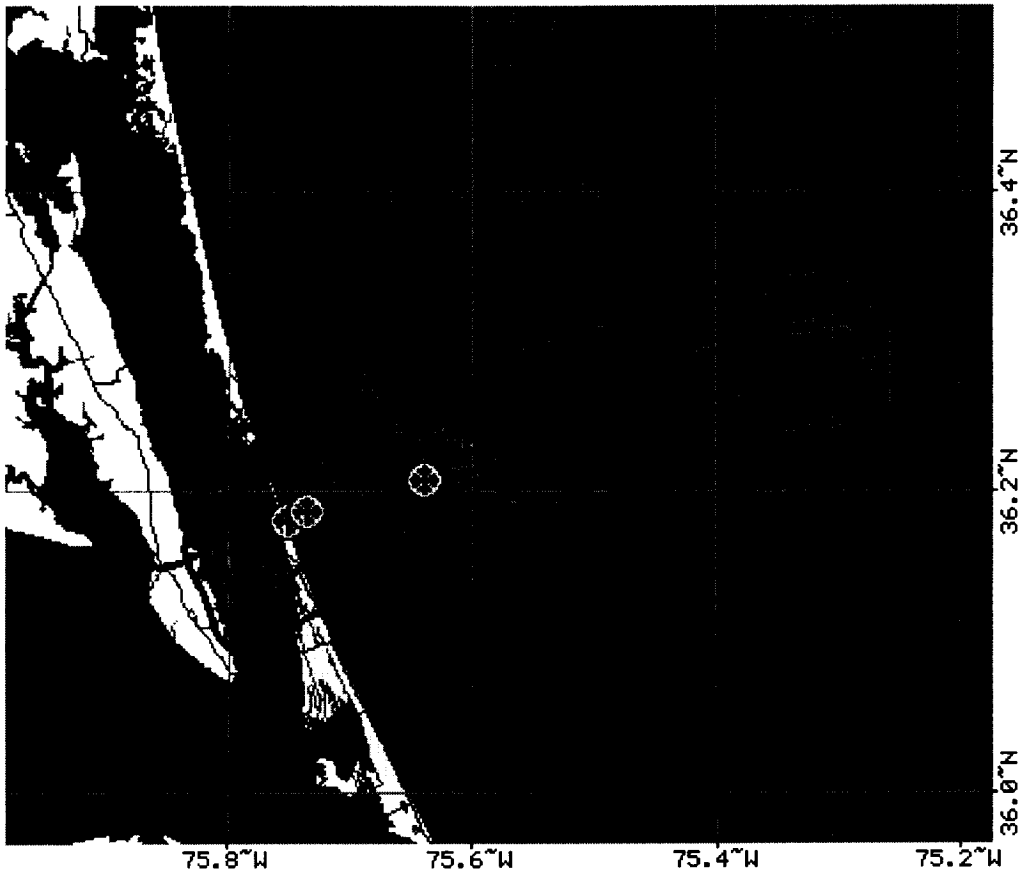

Fig. 4. EOPACE Experiment Flight Path

experiment conducted by the Virginia Space Grant Consortium (VSGC). This experiment collected data which first mapped the altitude dependence of the reflected signal waveform shape [9].

On all of these aircraft flights, an Ashtech Z-12 survey receiver was also carried. Differential corrections were used with post-processing software to determine the aircraft flight path very accurately from this receiver. Precise GPS ephemerides from the National Geodetic Survey [18] were also obtained for the days of the flights.

III. Post Processing

POST processing was performed on the raw, or level 0 data from the receiver which accomplishes two basic functions: determining the location of the specular reflection point on the surface of the ellipsoidal Earth, and re-alignment of each (1/2 code chip spaced) correlator sample in code delay relative to the specular point. This was done to more precisely reference the measurement to the location of ground truth (the location of the specular point can be several kilometers from the aircraft ground track) and to continuously map the waveform samples at finer than 1/2 chip precision.

This realignment was performed through use of the navigation data from the aircraft and the NGS ephermides. Timing of the measurements was either provided from the GPS solution (in the case of 4 or more direct satellites tracked), or from a single satellite in the case of the PDMR. The true path length difference of a specular reflection from the surface of the WGS-84 ellipsoid was computed by minimizing the total path length of a reflected signal.

$$\rho_L = \sqrt{\begin{array}{l}(X_L - X_S(\phi_S, \lambda_S))^2 + \\ (Y_L - Y_S(\phi_S, \lambda_S))^2 + \cdots \\ (Z_L - Z_S(\phi_S, \lambda_S))^2\end{array}} + \sqrt{\begin{array}{l}(X_{GPS} - X_S(\phi_S, \lambda_S))^2 + \\ (Y_{GPS} - Y_S(\phi_S, \lambda_S))^2 + \\ (Z_{GPS} - Z_S(\phi_S, \lambda_S))^2\end{array}} \tag{3}$$

The Earth-centered Earth-fixed coordinates of the LHCP antenna phase center (X_L, Y_L, Z_L) were obtained from the differentially corrected Ashtech flight path (assuming level flight). The GPS satellite

coordinates $(X_{GPS}, Y_{GPS}, Z_{GPS})$ were obtained from the NGS ephemeris. The coordinates of the specular point (X_S, Y_S, Z_S) were found by numerically minimizing ρ_L through varying the geodetic latitude and longitude, ϕ_S and λ_S of a specular point which was assumed to be fixed to lie on the WGS-84 ellipsoid. The details of these coordinate systems can be found in [11].

The difference between this geometric location of the specular point and the stored code phase information from sampling the code epoch for each correlator was used to compute the relative delay between each power sample and the specular point.

This alignment is illustrated in figure 5 (a) and (b).

The correlation power was then normalized to have a constant total area of one half code chip by dividing by the total integrated power in all range bins at each waveform sample. This removes changes in the intensity of the incident radiation and was also found to produce results with the lowest variance. This effectively eliminates the need to calibrate the lower channel correlation values with a physically meaningful measurement of reflected power and eliminates many uncalibrated effects such as aircraft attitude motion and the antenna gain pattern.

The result of post-processing is a standard set of "level 1" data. This consists of waveform measurements of the incoherent power, $Y_k^2(\delta_i)$ at specific code delays, $\delta_{k,i}$. For each k^{TH} waveform sample (taken at a 1Hz rate for the SDMR and a 10 Hz rate for the PDMR) auxiliary information giving the specular point location (ϕ_{S_k}, λ_{S_k}) and the GMT of the measurement are also tabulated.

These waveform samples were then used with several retrieval techniques to estimate surface wind speed. In this paper, summaries are provided for two of these techniques.

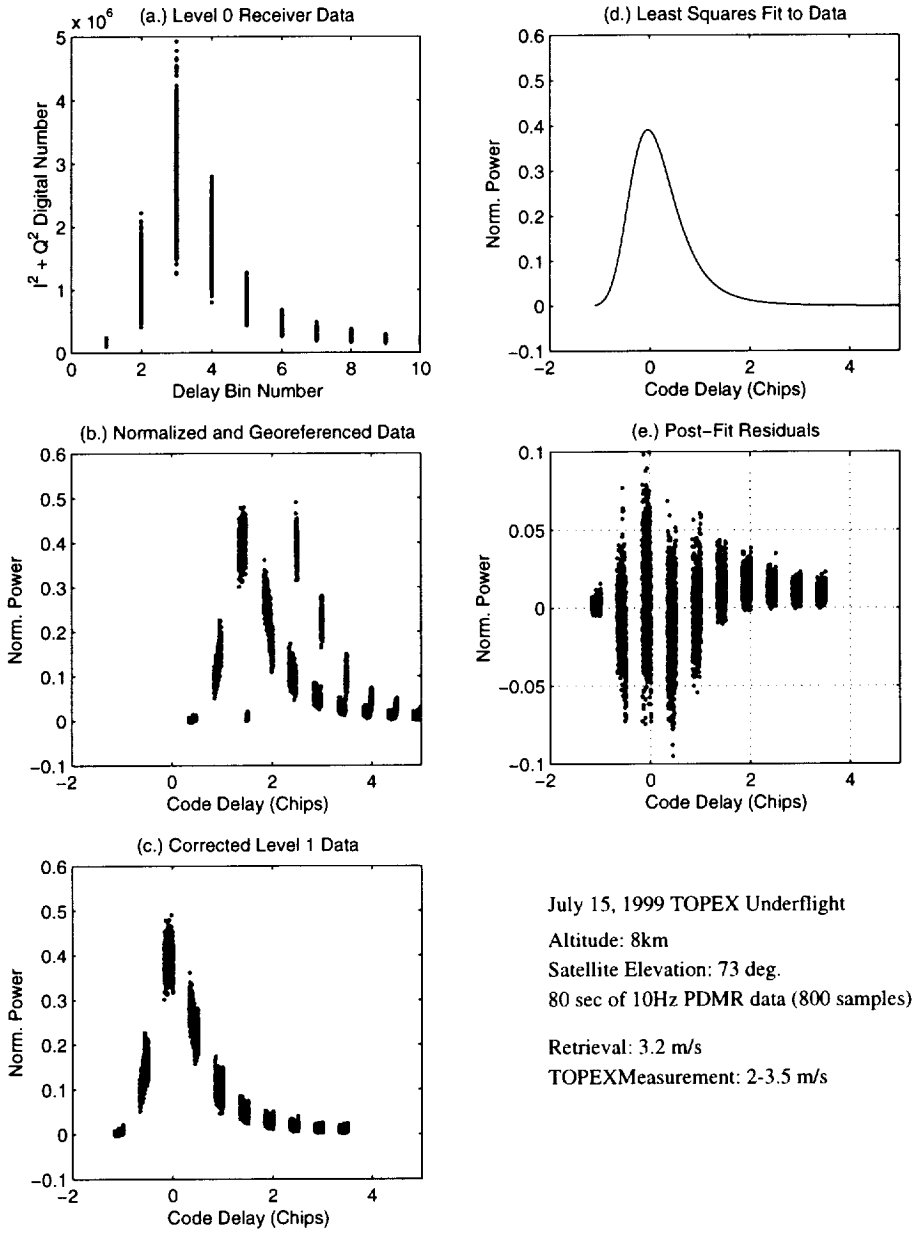

Fig. 5. Example Data Post Processing

IV. Estimation Techniques

A. Wind Speed Estimation Using the Waveform Trailing Edge

This retrieval technique includes the generation of sets of modeled waveforms, the normalized power versus time delay with respect to the nominal specular point, for various wind speeds. The theoretical model by Zavorotny and Voronovich [6] was used to generate waveforms. The model used the elevation spectrum of wind-driven sea surface derived by Elfohaily et al. [12] taking into account fetch-limited conditions. For this research, we assumed that seas are well-developed with an unlimited fetch. The trailing edge of the waveform taken in a logarithmic scale was used for the estimation as the most sensitive part to surface wind speeds.

The measured signals were normalized by the integral power observed in delay bins within the expected range of the glistening zone. Measurements showed that there is no strong signal correlation between the top and bottom channels. The total reflected power is not expected to depend on surface statistics and can be used as a normalization factor.

A comparison was made between data collected at 3.8 km altitude on the EOPACE experiment and the theoretical model developed by Zavorotny and Voronovich. To smooth this data, a 150 second sliding average was applied to the raw reflected GPS measurements. As described above, an adaptive signal normalization, which generates a constant area waveform was used to cancel out the uncalibrated effects of antenna gain, aircraft attitude motion, and difference in cable loss and front-end gain between the direct and reflected signals. This data was "binned" across discrete code delays measuring one half-code chip. (This corresponds to 150 meters in range resolution). To account for variations in

the noise floor of the reflected signal, the correlation power recorded in the last four delay bins and subtracted it from the reflected signal. The trailing edge slope on a decibel scale was estimated with a least squares fit of a straight line to the measured waveforms between 5 and 20 dB. This was compared to the theoretical model predictions using various incremental wind speeds. The estimated wind speed was obtained by interpolating the measured slopes between the modeled ones.

The TOPEX-altimeter over-flight covered a wide range of wind speeds ranging from 0.5 m/s to 8.7 m/s within a ground distance of about 40 km. After processing the data, the TOPEX-indicated geographic area was matched with the location of GPS measurements. Two different waveforms for PRN15 were obtained for 0.5 and 8.7 m/s wind speeds as indicated in Figure 6. This figure displays the modeled values for these two different wind speeds. As predicted by the model, a higher wind speed results in a wider waveform with a lowered peak power. Note that agreement between measured and modeled waveforms can be assessed on the trailing edge of the waveform between 5 and 20 dB as described earlier. The measured and modeled wind speeds showed good agreement for PRN15 in Figure 7.

It can be concluded that for the lower 0.5 m/s wind speed, the agreement appeared not to be as good as for the 8.7 m/s wind speed. This could be due to the fact that at lower wind speed the Rayleigh criteria of diffuse scattering may be violated, possibly limiting the accuracy of modeled waveform at lower than 2 to 3 m/s wind speeds. In Figure 7, we displayed the processed waveform for PRN19 along with the predicted waveforms for 6, 8, 10, and 12 m/s. TOPEX wind measurement indicated an 8.7 m/s. The figure clearly shows that the observed wind speed is between 8 and 10 m/s. We have found the trailing edge of the waveform to be very stable between 5 and 20 dB , therefore we used

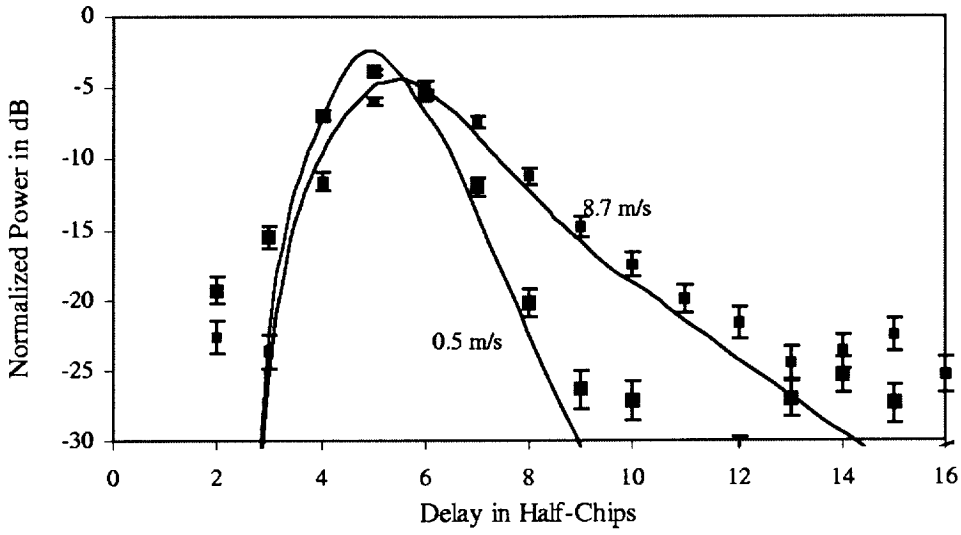

Fig. 6. Predicted and measured waveforms for low and high wind speeds for PRN15

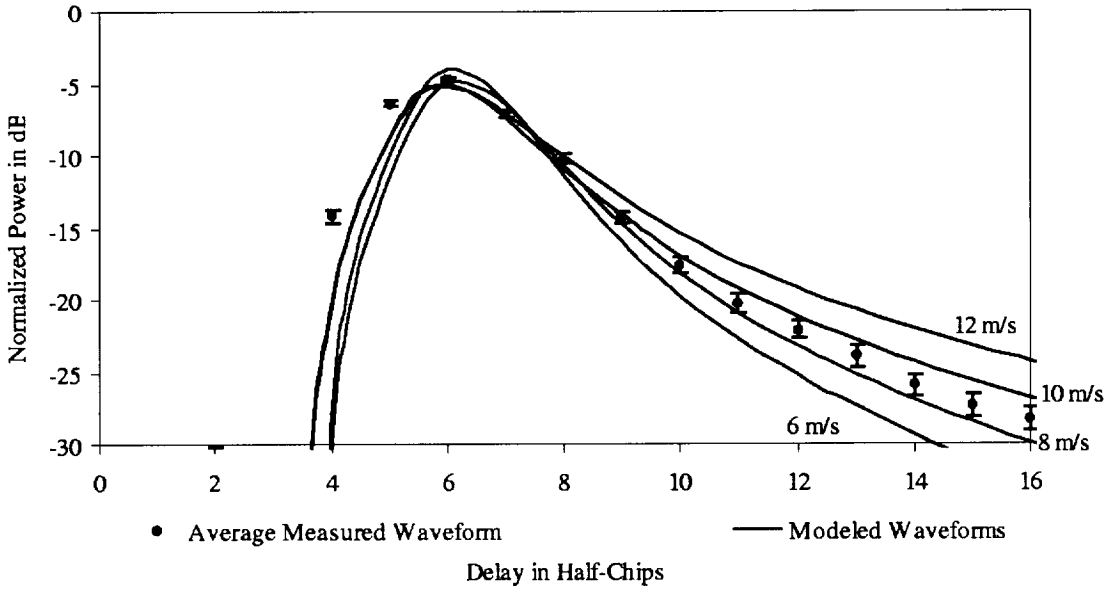

Fig. 7. Predicted and measured waveforms for 8.7 m/s wind speed (PRN19)

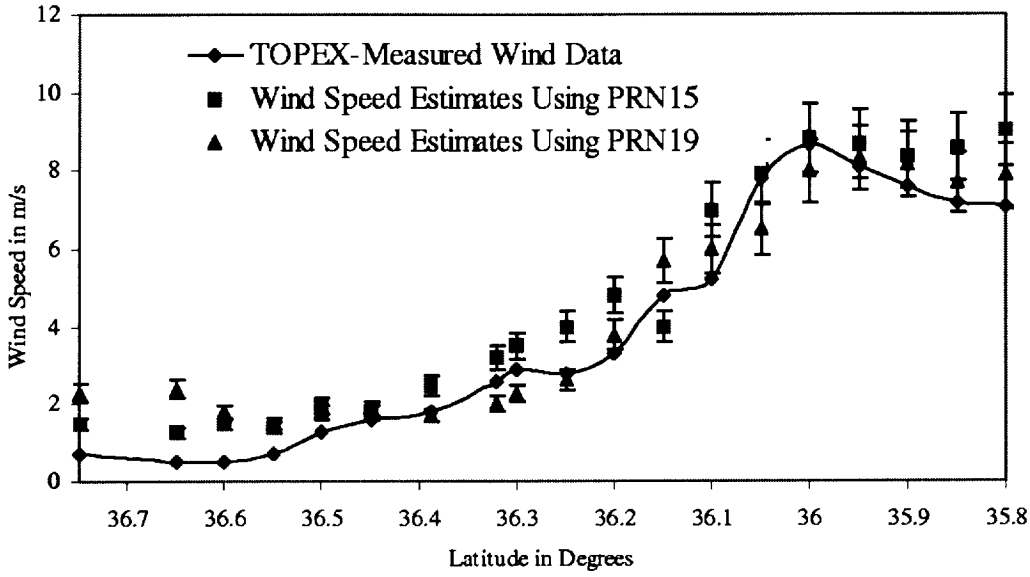

Fig. 8. Estimated wind speed using PRN15 and PRN19 and TOPEX ground truth

that region to routinely infer surface wind speeds.

For every TOPEX wind speed measurement, the trailing edge slope was estimated using the measured waveforms between 5 and 20 dB and the theoretical model using various incremental wind speeds. The estimated wind speed was obtained by interpolating the measured slopes between the modeled ones. In Figure 8, we displayed both the TOPEX measured wind speeds and our estimated ones using GPS data from two different satellites: PRN15 and PRN19. The $1-\sigma$ error bars were also displayed for the measured wind speeds. The figure shows that the error bars are larger for higher wind speed. This is due to the fact that for higher wind speeds the separation between two waveform slopes, corresponding to two separate wind speeds, are smaller than the separation between two wind speeds at smaller wind speeds. Furthermore, the figure indicates that wind speeds estimated independently using the two satellites show good agreement with the TOPEX-measured wind data.

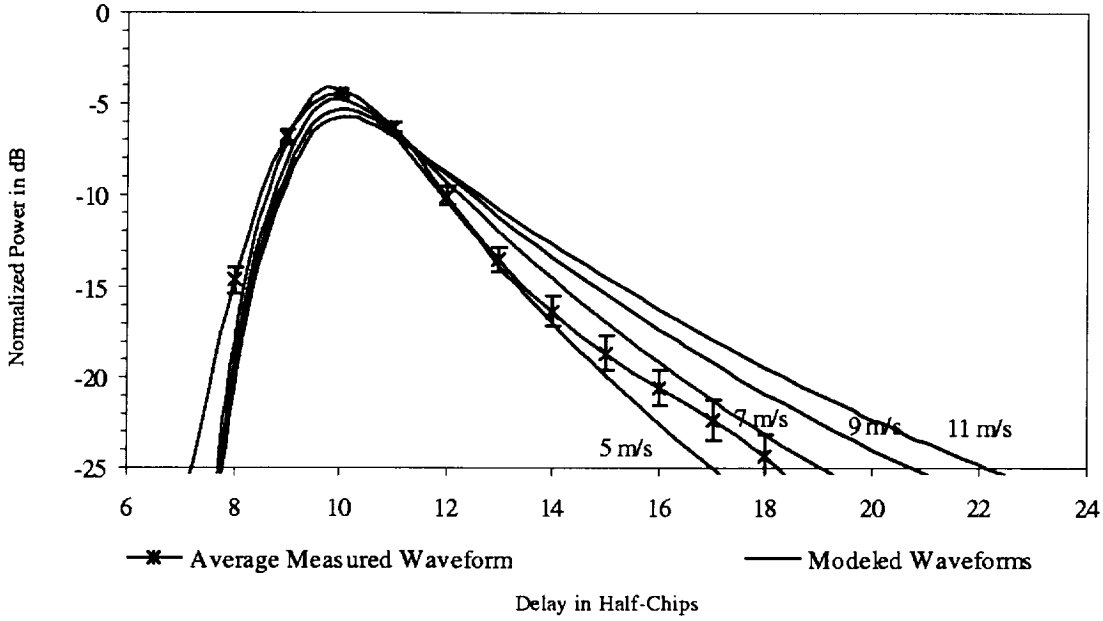

Fig. 9. Predicted and Measured Waveforms for PRN04 at 6.5 km altitude.

We have also processed the surface-reflected GPS data from the VSGC Balloon Experiment. Here, waveforms are presented for three different altitudes for the same PRN04 satellite. In Figure 9, a waveform for PRN04 collected at an altitude of 6.5 km is shown. The modeled theoretical waveforms for wind speeds 5, 7, 9, 11 m/s are also plotted. Figure 10 presents a waveform for the altitude 12 km, whereas Figure 11 displays the highest altitude of 25 km. The comparison of these figures reveal that the waveform trailing edge slope and peak power decreases with height as predicted by the theoretical model. A comparison between modeled and measured waveforms suggests that the wind speed might have been between 5 to 7 m/s around that region. The nearby buoy data indicates a 5 m/s wind speed for the vicinity of the experiment. Even at 25 km altitude a strong reflected signal was observed showing a straight line trailing edge (on a logarithmic scale) allowing the estimation of surface wind

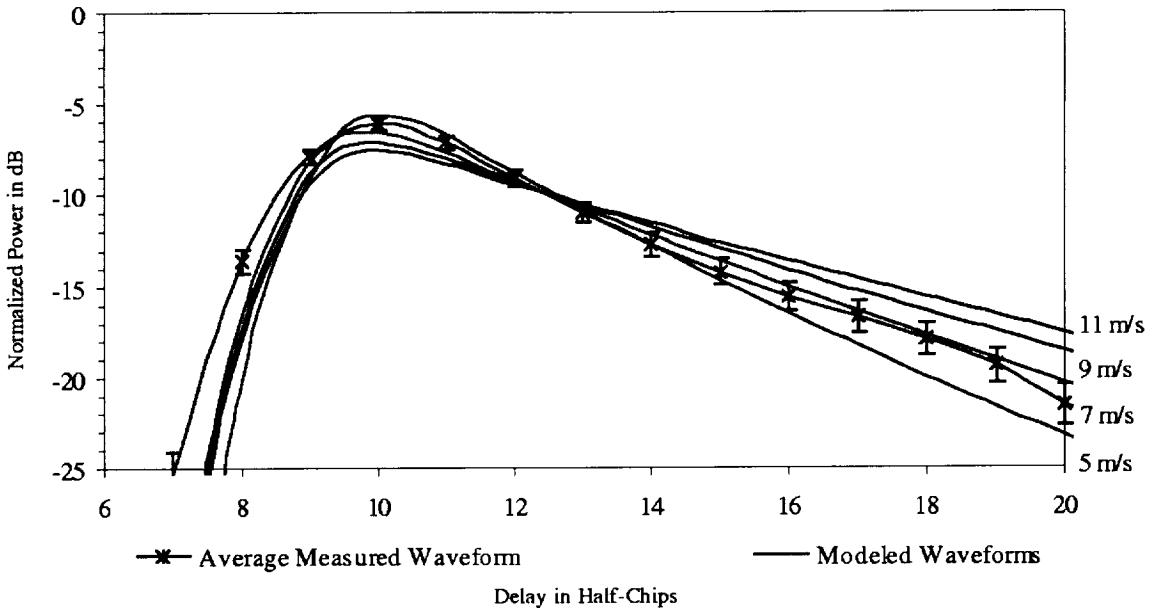

Fig. 10. Predicted and Measured Waveforms for PRN04 at 12 km altitude.

speed. These results show that similar estimates of 5 m/s wind speed were obtained at three different altitudes up to 25 km.

B. Series Approximation of Waveform Shape

Conceptually, existing analytical models [6] and [4] generate waveforms, $Y^2(\delta)$, with a function relationship to wind speed.

$$Y^2(\delta) = f(\delta, V_w) \tag{4}$$

Only the magnitude of wind speed (V_w) was considered in this study. The use of the anisotropic surface statistics [6] (or a skewed non-Gaussian probability density function) [4] would show that the waveform shape is weakly dependent upon wind direction as well. It has not been determined if this

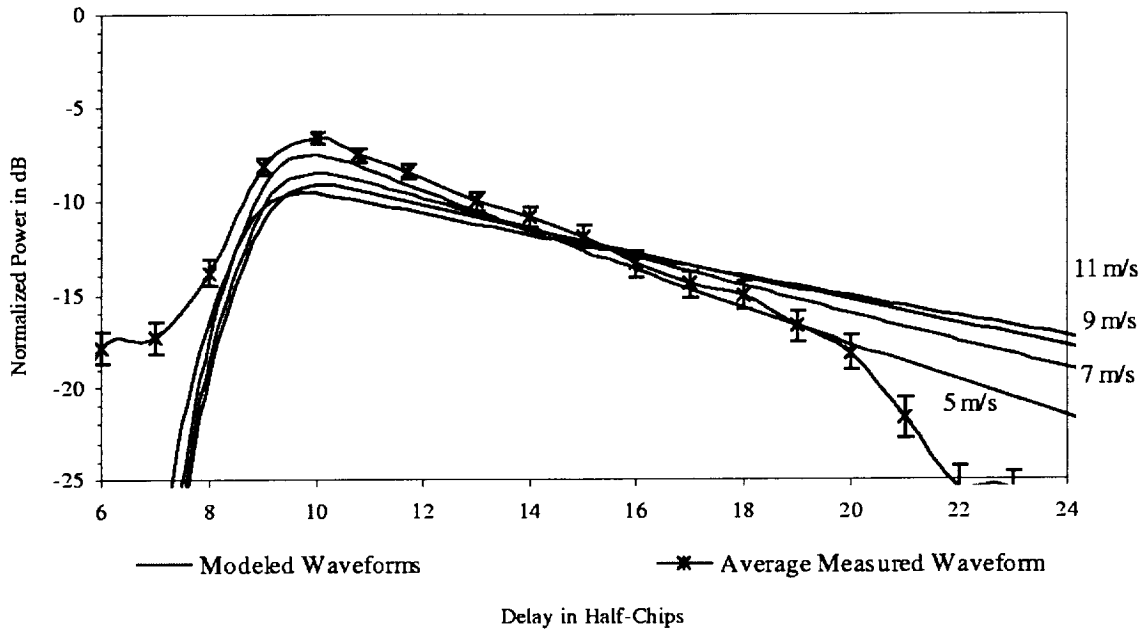

Fig. 11. Predicted and Measured Waveforms for PRN04 at 25 km altitude.

dependence is strong enough to obtain any useful retrievals of wind direction from waveform data alone.

The practical computation of the cross-correlation in equation 2 requires three integrals: Two over the surface to compute the power per delay, $p(\eta)$, and one for the convolution of reflected power with the Λ^2 function. This cannot be analytically inverted. Furthermore, because the measurements were made in the presence of noise, it was best to use an estimator on an overdetermined set of measurements optimally combined such that the statistical error in the state estimate is minimized. This required that this triple integral be computed for each measurement point, on multiple iterations to generate the innovations process that was used to update the state estimate. Performing the complete integration for each point would have been computationally prohibitive. For that reason, this integration was

approximated by a finite series expansion in terms of wind speed (V_w) and code delay (δ) having the following form.

$$Y^2(\delta) \approx S \exp\left[\sum_{i=0}^{N}\sum_{j=0}^{M} a_{i,j} V_w^j (\delta - \delta_0)^i\right] \tag{5}$$

An 8th order series of this form was found to make a very good approximation to the shape of the waveform. It should be noted that the Λ^2 function in this convolution is discontinuous and no continuous function is expected to approximate it very well near the peak. The coefficients were determined by a best fit to the model of Clifford, et al., [13] which uses the Apel wave spectrum [14]. For the range of winds from 6 to 10 m/s various wave spectra produce close results, as is shown in Komjathy, et al. [15] by comparing waveform shapes generated using both Apel and Elfouhaili spectra. Three states: wind speed V_w delay of the peak of the waveform from the computed specular point, δ_0 and the scale factor S were then estimated using the above form as the observation equation. A nonlinear least squares estimator was then applied using segments of waveform data (δ_k, Y_k^2).

A constant noise floor, determined using the theoretical value set by the AGC prior to digital sampling was subtracted from all correlation measurements before the constant area normalization was performed.

Although each waveform sample was scaled to have a constant area of one half chip, the scale factor (S) was found to improve the estimation accuracy. The reason for this was postulated to be that a finite number of delay bins do not record the complete waveform because portions of the trailing edge often extend beyond the range of these bins. The scale factor therefore accounts for the fact that the measured waveform, once scaled to be constant area, has slightly larger area than that predicted by

theory. Using the state δ_0 effectively calibrated the relative delay between the direct and the reflected signal path lengths. The variance in this state could also being interpreted as an upper bound on the practical accuracy achievable using the reflected GPS signal as an altimeter. The state estimate in figure 12 suggests that this uncertainty is approximately 0.1 chip, or 30 meters. Figure 12 shows the time history of these three states for a typical segment of reflected GPS data collected under the TOPEX ground track.

Three effects and receiver anomalies were not accounted in these signal models. These were identified and corrected before the data was processed by the least squares estimator. Editing the data in this manner was found to improve the performance of this estimator and removed most of the outlying wind speed estimates. However, as the single outlier point in the estimate for δ_0 near -73.4 deg. in figure 12 shows, there were occasionally these anomalies which were not detected. With an improved residual monitoring process these cases may be eliminated in the future. First, the total power in all delay bins was computed and if this fell below a threshold, then the complete waveform was rejected. This eliminated measurements made over land, and time in which the receiver had not acquired a strong reflected signal. Second, occasionally slips by an integer number of half code chips in the spacing of the delay bins was observed (as demonstrated by the two superimposed waveforms on figure 5 (b)). This anomaly was identified and corrected by adding or subtracting an integral number of half-code chips to the array of delay variables (δ) on each waveform until the maximum recorded cross correlation measurement was within 1 code chip of the specular reflection point. This correction is illustrated in figure 5 (c). The outlier shown near -73.4 deg. was the result of failure to detect one of these slips. An improved receiver design (to eliminate this failure at the source) combined with a better residual

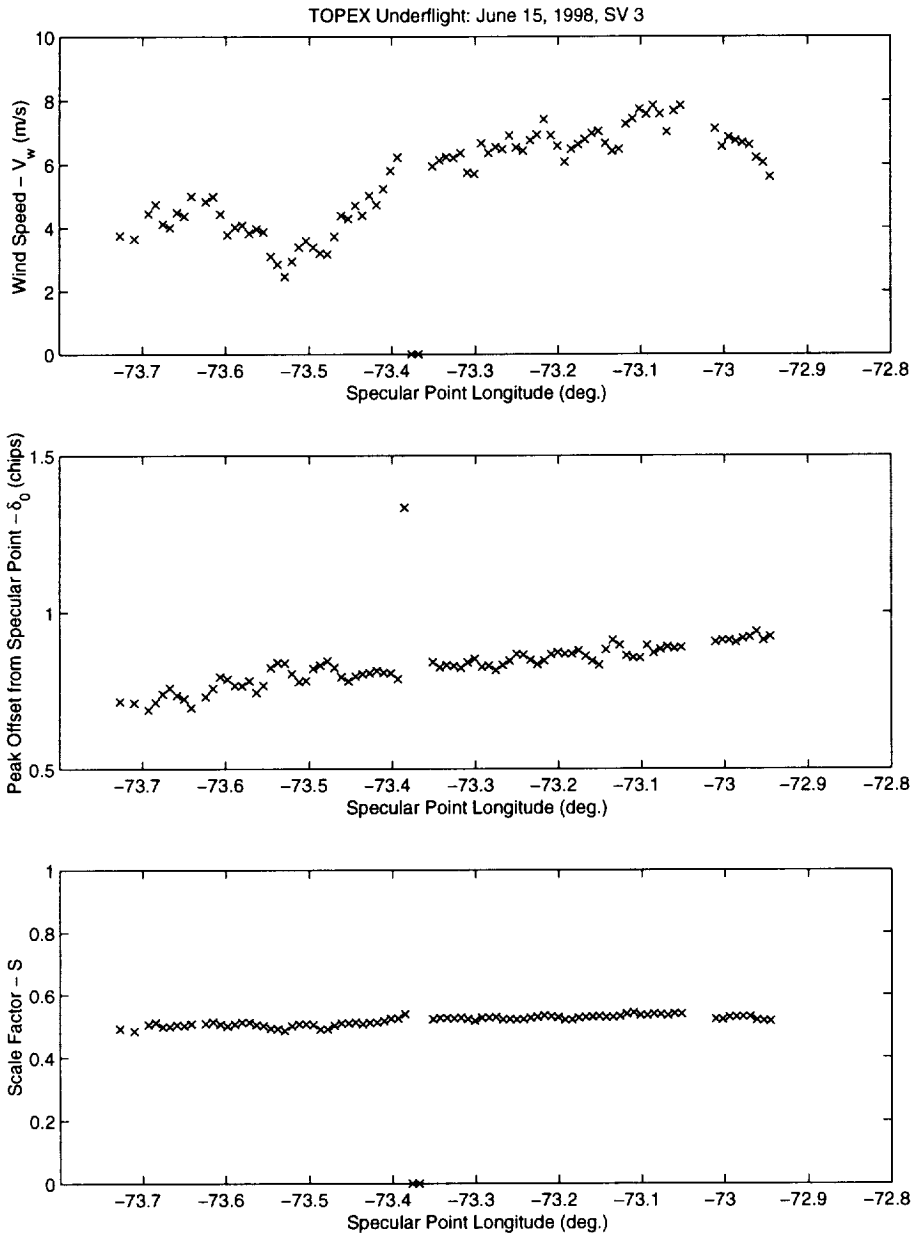

Fig. 12. Example State Estimates for Wind Speed Retrieval

monitoring process could reduce these cases.

The third effect identified was another receiver artifact in which the leading edge of the waveform extended earlier than the first correlator. In these cases, there was correlation power in the earliest correlator power bin. Attempts to blindly fit the function defined above to this situation resulted in a wider than required waveform shape and consequently a higher wind speed. Individual waveforms in which this correlation power exceeds some threshold are deleted from the ensemble. Although most of the information about the surface slope statistics is contained in the trailing edge of the waveform, this method makes use of the complete shape and the presence of this anomaly resulted in higher than expected wind speed estimates because of the tendency to fit a "wider" function to waveforms truncated in this manner. At present all that was done to correct for this effect is to delete the waveform sample from the ensemble altogether. It may be possible to include zero-valued power measurements at time delays earlier than the start of the measurements so as to force the curve fitting algorithm to converge to zero for delays earlier than -1 code chip relative to the specular point. This correction would be justified because no reflected power could be received earlier than the specular point and therefore no correlation could exist earlier than 1 chip prior to the specular point. Methods described earlier which use only the trailing edge data would not suffer from this anomaly.

Finally, a residual monitoring process is used in which a threshold is set on the sum square of residuals in one waveform. This was computed from the difference between the observed and computed power following the least squares estimate for the k^{TH} waveform.

$$r_k = \sum_i (Y_{k,i}^2 - Y_c(\delta_{k,i}, V_w, S, \delta_0))^2 \tag{6}$$

in which Y_c is the function from equation (5) computed with the estimated state vector (V_w, S, δ_0). The k^{TH} waveform was rejected from the ensemble when r_k exceeded a threshold. The complete ensemble (less the waveforms which were rejected) was then processed through the least squares estimator a second time. Figure 5 (d) shows the resulting best fit waveform to the data from figure 5 (c). Figure 5 (e) shows the post fit residuals for each measured waveform.

Results from this estimator were compared against the TOPEX wind speed retrievals for the series of TOPEX underflights and against the surface truth measured from buoys during the EOPACE experiment. Figure 13 shows a comparison between the results of this method operating on PDMR data and TOPEX wind speed retrieval. These retrievals were performed on 100 second batches of waveform measurements using coefficients, $a_{i,j}$ computed for the altitude and average elevation of each GPS satellite from which data was collected. Longitude of the TOPEX ground track and the specular point are used as the independent variable. These results indicate at most a 2 m/sec difference between the two sensors. It should be noted in this comparison that the longitude of the reflection specular point does not lie on exactly the same line as the TOPEX ground track and that measurements at the same longitude from the two sensors are not necessarily the physically closest on the ocean surface. This could explain the apparent shift between the two retrievals on the May 5 data. Also, the largest discrepancies between the two sensors occur for low wind speeds ($\leq$2 m/s), showing a similar effect to that observed in the trailing edge slope retrieval.

For the EOPACE experiment, segments of data in which the specular point of the reflection was near to the three sources of surface truth were used for this comparison. Please refer back to figure 4 for the location of the ground tracks for these two flights. Measurements with a specular point longitude

of less than 75.7 deg.W were not used because these were judged to lie too close to the shore line. Measurements from these points were often significantly lower than that from the recording buoys. The Met Buoy was 10 km from the shore and was expected to give the best comparison with nearby measurements. The land area surrounding the shoreline was relatively flat, however, and therefore the wind speed measured at all three surface truth locations was found to be similar. Wind direction was obtained from the Duck meteorological station.

For retrievals of the EOPACE data, batches of 300 seconds of waveform data were processed for each state estimate. A set of coefficients $a_{i,j}$ were computed for and altitude of 3.8 km and elevation increments of 15 degrees. The set for the elevation closest to the average elevation for a given satellite was used in the estimator. This simplification was justified because the shape of the waveform is not strongly dependent upon grazing angle for the satellite elevations used.

Results from this are shown in figures 14 through 17. The comparison data from the Flux and Met research buoys was averaged for 5 minutes near the time of each overpass. The standard deviation of this measurement is also illustrated by the errorbars on these figures. Duck wind speed measurement was taken as the average of the three measurements recorded nearest recorded time to the overflights.

These plots show in most cases an agreement to better than 2 meters per second between the reflected GPS retrievals and the surface truth data.

V. CONCLUSIONS AND FUTURE WORK

These experiments have demonstrated reliable retrievals of geophysical data using the power versus delay waveform recorded from bistatically scattered GPS signals. The two airborne data campaigns

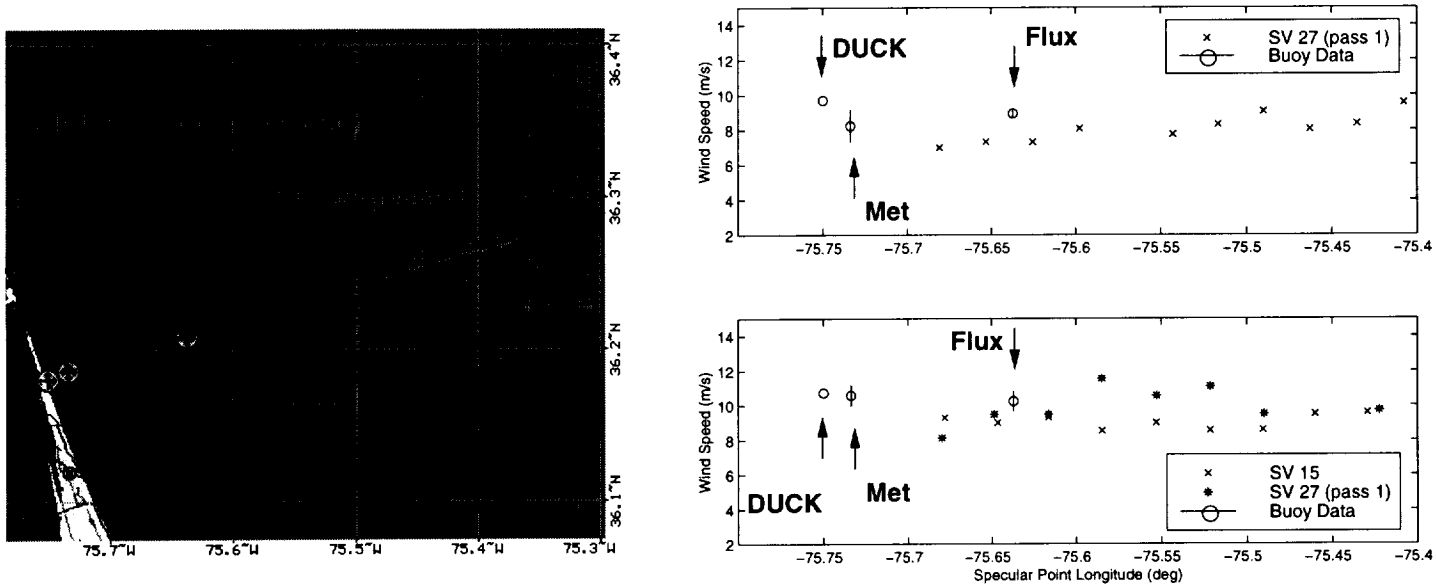

Fig. 14. EOPACE Data Comparison: March 1, 1999

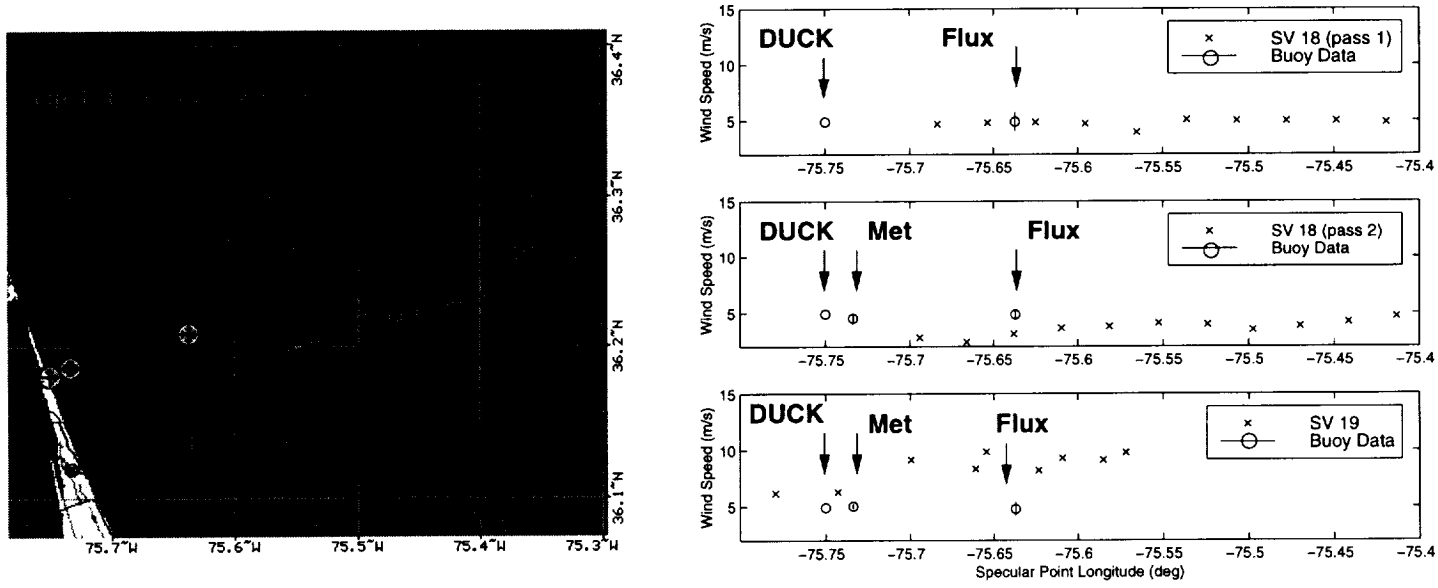

Fig. 15. EOPACE Data Comparison: March 5, 1999

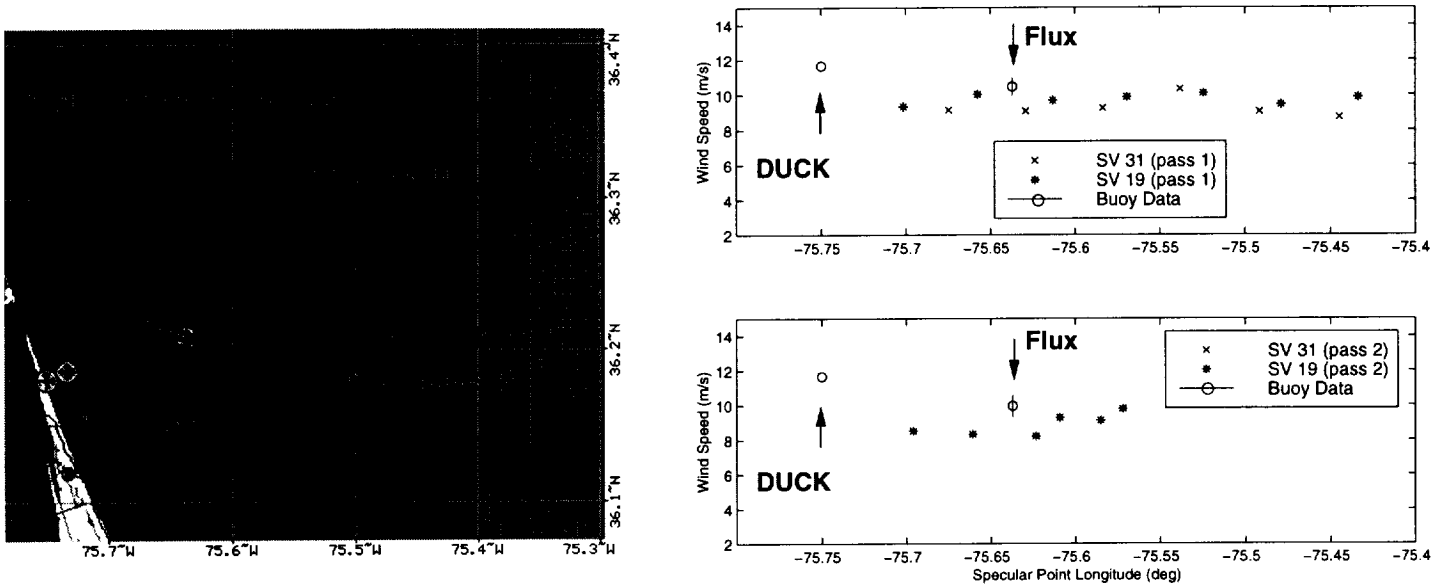

Fig. 16. EOPACE Data Comparison: March 8, 1999

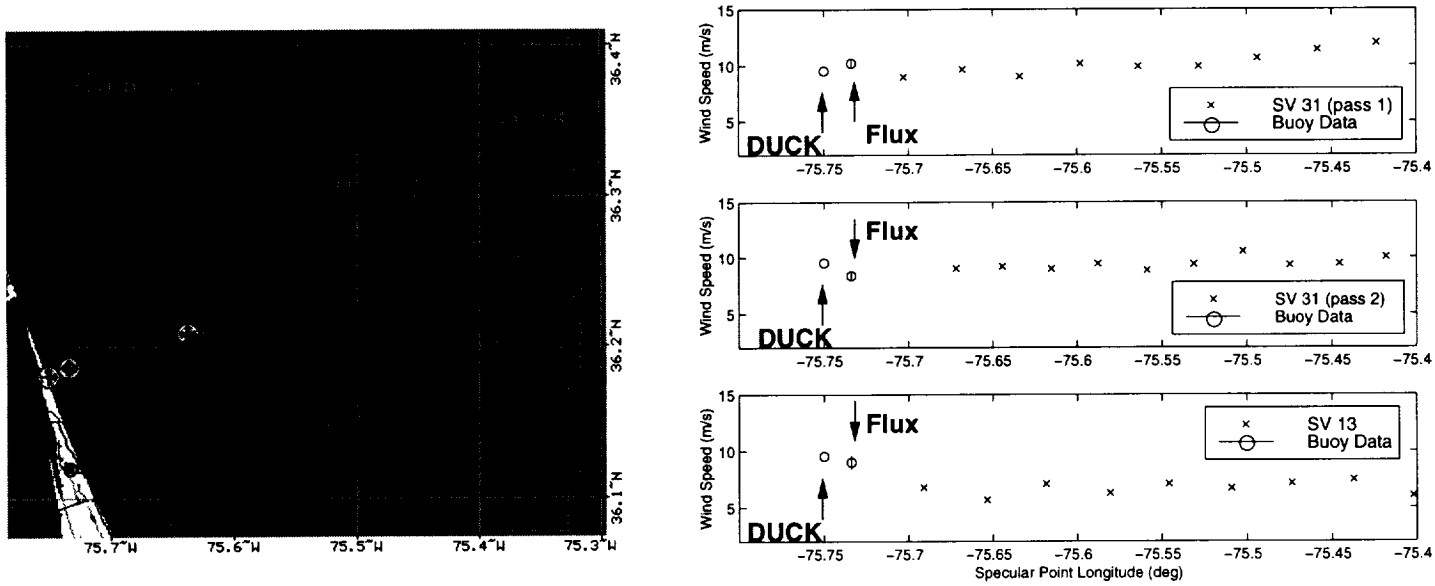

Fig. 17. EOPACE Data Comparison: March 12, 1999

evaluated in this study provide reference data to compare retrieval techniques. Future experimentation, however, should be conducted under better known conditions and with better ground truth. Retrieval methods could be improved through better electromagnetic models of the reflection process, specifically effects of polarization. Also, statistical parameters describing the random rough surface could be used as the estimation state as opposed to a geophysical parameter such as wind speed. This separates the more fundamental geometric optics measurement model from the empirical relationship between geophysical data (wind vectors) and surface statistics (mean square slope and wave spectra). Another area of improvement is the incorporation of multiple satellites into the same estimator, for measurement situations in which the specular point locations are close enough together such that they can be assumed to be samples of the same surface process. An understanding of the statistics of the waveform power samples, from both experimental and theoretical sources, would improve the estimator design and provide a rational basis for selecting data weights and thresholds on the residual monitoring.

Directional information may also be retrieved from the reflected signal through the mapping of the waveform in both code delay and Doppler frequency. This would require enhancements in the receiver architecture and is the next step in the development of this hardware.

REFERENCES

[1] Katzberg, S. J., Garrison, J. L., Coffey, N. C., and Kowitz, H. R., *Method and System for Monitoring Sea State Using GPS*,application filed with the U.S. Patent and Trademark Office, 8 January 1998.

[2] Kaplan, Elliot D., ed., *Understanding GPS Principles and Applications*,Artech House Publishers, Boston, 1996.

[3] Parkinson, Bradford W., Spilker, James J., Axelrad, Penina, and Enge Per, eds. *Global Positioning System: Theory and Applications Volume I*,AIAA, Washington DC, 1996.

[4] Lin, B., Katzberg, S. J., Garrison, J. L., and Wielicki, B., The Relationship Between the GPS Signals Reflected from Sea

Surfaces and the Surface Winds: Modeling Results and Comparisons With Aircraft Measurements, *Journal of Geophysical Research - Oceans*,in press.

[5] Cox, C. and Munk, W., Measurement of the Roughness of the Sea Surface from Photographs of the Sun's Glitter, *Journal of the Optical Society of America*, Vol. 44, No. 11, pp. 838-850, November 1954.

[6] Zavorotny, V. U., and Voronovich, A.G., Scattering of GPS signals from the ocean with wind remote sensing application, *IEEE Trans. Geosci. Remote Sensing.*,in press.

[7] GEC Plessey Semiconductors, *Global Positioning Products Handbook*,August 1996.

[8] Garrison, J. L., Katzberg, S. J. and Hill, M. I., Effect of Sea Roughness on Bistatically Scattered Range Coded Signals from the Global Positioning System, *Geophysical Research Letters*, Vol. 25, No. 13, pp. 2257-2260, July 1, 1998.

[9] Garrison, James L., and Katzberg, Stephen J., "The Application of Reflected GPS Signals to Ocean Remote Sensing," *Remote Sensing of Environment*, in press.

[10] National Oceanic and Atmospheric Administration (NOAA), NDBC Data Availability Summary, NDBC Technical Document 96-03, Stennis Space Center, MS, February 1997.

[11] Hofmann-Wellenhof, B., Lichtenegger, H., and Collins, J., *GPS Theory and Practice*,Springer-Verlag, New York, 1992.

[12] Elfouhaily, T., B. Chapron, K. Katsaros, and D. Vandermark, "A Unified Directional Spectrum for Long and Short Wind-Driven Waves," *J. Geophys. Res., 102*,15,781-15,796.

[13] Clifford, S.F., V.I.Tatarskii, A. G. Voronovich and V.U.Zavorotny, "GPS Sounding of Ocean Surface Waves: Theoretical Assesment,in *Proceedings of the IEEE International Geoscience and Remote Sensing Symposium: Sensing and Managing the Environment*,pp. 2005-2007, IEEE, Piscataway, N. J., 1998.

[14] Apel, John R., "An Improved Model of the Ocean Surface Wave Vector Spectrum and its Effects on Radar Backscatter," *Journal of Geophysical Research*, Vol. 99, No. C8, August 15, 1994, pp. 16,269-16,291.

[15] Komjathy, A., Zavorotny, V., Axelrad, P., Born, G. H., and Garrison, J. L., GPS Signal Scattering from Sea Surface: Wind Speed Retrieval Using Experimental Data and Theoretical Model, *Remote Sensing of Environment*, in press.

[16] Garrison, J. L., Katzberg, S. J., and Howell, C. T., Detection of Ocean Reflected GPS Signals: Theory and Experiment, *Proceedings IEEE Southeastcon*, Blacksburg, VA, p. 290-294, 12-14 April 1997.

[17] Graf, J., Sasaki, C., Winn, C., Lui, W. T., Tsai, W., Freilich, M., and Long, D., NASA Scatterometer Experiment, *ACTA Astronautica*,Vol. 43, No. 7, pp 367-407, 1998.

[18] National Oceanic and Atmospheric Administration (NOAA), NOAA Technical Report NOS 133 NGS 46, Extending the National Geodetic Survey Standard Orbit Formats, November 1989

[19] Shaw, Joseph A., Churnside, James H., "Scanning-laser Glint Measurements of Sea-Surface Slope Statistics," *Applied Optics*,Vol. 36, No. 18, June 1997, pp 4202-4213.